









## Pragmatic algorithm for visual assessment of 4-Repeat tauopathies in [<sup>18</sup>F] PI-2620 PET Scans

Theresa Bauer<sup>a,1</sup>, Matthias Brendel<sup>a,b,e,1</sup> , Mirlind Zaganjori<sup>a</sup> , Alexander M. Bernhardt<sup>b,c,e</sup> ,  
 Alexander Jäck<sup>b,c</sup>, Sophia Stöcklein<sup>d</sup>, Maximilian Scheifele<sup>a</sup>, Johannes Levin<sup>b,c,e</sup>,  
 Thilo van Eimeren<sup>f,g</sup>, Alexander Drzezga<sup>f,g,h</sup>, Osama Sabri<sup>i</sup> , Henryk Barthel<sup>i</sup>,  
 Robert Perneczky<sup>b,e,j,k,l</sup>, Günter Höglinger<sup>b,c,e</sup> , Nicolai Franzmeier<sup>e,m,n</sup>,  
 Johannes Gnörich<sup>a,b,\*</sup> , German Imaging Initiative for Tauopathies (GII4T)

<sup>a</sup> Department of Nuclear Medicine, University Hospital, LMU Munich, Munich, Germany

<sup>b</sup> German Center for Neurodegenerative Diseases (DZNE) Munich, Munich, Germany

<sup>c</sup> Department of Neurology, University Hospital, LMU Munich, Munich, Germany

<sup>d</sup> Department of Radiology, University Hospital, LMU Munich, Munich, Germany

<sup>e</sup> Munich Cluster for Systems Neurology (SyNergy), Munich, Germany

<sup>f</sup> Department of Nuclear Medicine, Faculty of Medicine and University Hospital Cologne, Cologne, Germany

<sup>g</sup> German Center for Neurodegenerative Diseases (DZNE), Bonn/Cologne, Germany

<sup>h</sup> Institute of Neuroscience and Medicine (INM-2), Molecular Organization of the Brain, Forschungszentrum Jülich, Germany

<sup>i</sup> University Hospital Leipzig, Department of Nuclear Medicine, Leipzig, Germany

<sup>j</sup> Department of Psychiatry and Psychotherapy, University Hospital, LMU Munich, Munich, Germany

<sup>k</sup> Sheffield Institute for Translational Neuroscience (SITraN), University of Sheffield, Sheffield, UK

<sup>l</sup> Ageing Epidemiology Research Unit (AGE), School of Public Health, Imperial College London, London, UK

<sup>m</sup> Institute for Stroke and Dementia Research, LMU Munich, Munich, Germany

<sup>n</sup> University of Gothenburg, The Sahlgrenska Academy, Institute of Neuroscience and Physiology, Department of Psychiatry and Neurochemistry, Mölndal and Gothenburg, Sweden

### ARTICLE INFO

#### Key words:

Visual read  
 Tauopathies  
 Tau-PET  
 Reading algorithm

### ABSTRACT

**Aim:** Standardized evaluation of [<sup>18</sup>F]PI-2620 tau-PET scans in 4R-tauopathies represents an unmet need in clinical practice. This study aims to investigate the effectiveness of visual evaluation of [<sup>18</sup>F]PI-2620 images for diagnosing 4R-tauopathies and to develop a straight-forward reading algorithm to improve objectivity and data reproducibility.

**Methods:** A total of 83 individuals with [<sup>18</sup>F]PI-2620 PET scans were included. Participants were classified as probable 4R-tauopathies ( $n = 29$ ), Alzheimer's disease (AD) ( $n = 20$ ),  $\alpha$ -synucleinopathies ( $n = 15$ ), and healthy controls ( $n = 19$ ) based on clinical criteria. Visual assessment of tau-PET scans (choice: 4R-tauopathy, AD-tauopathy, no-tauopathy) was conducted using either 20–40-minute or 40–60-minute intervals, with raw (common) and cerebellar grey matter scaled standardized reading settings (intensity-scaled). Two readers evaluated scans independently and blinded, with a third reader providing consensus in case of discrepant primary evaluation. A regional analysis was performed using the cortex, basal ganglia, midbrain, and dentate nucleus. Sensitivity, specificity, and interrater agreement were calculated for all settings and compared against the visual reads of parametric images (0–60-minutes, distribution volume ratios, DVR).

**Results:** Patients with 4R-tauopathies in contrast to non-4R-tauopathies were detected at higher sensitivity in the 20–40-minute frame (common: 79%, scaled: 76%) compared to the 40–60-minute frame (common: 55%, scaled: 62%), albeit with reduced specificity in the common setting (20–40-min: 78%, 40–60-min: 95%), which was ameliorated in the intensity-scaled setting (20–40-min: 91%, 40–60-min: 96%). Combined assessment of multiple brain regions did not significantly improve diagnostic sensitivity, compared to assessing the basal ganglia alone

\* Correspondence author at Marchioninistrasse 15, 81377, Munich, Germany

E-mail address: [Johannes.Gnoerich@med.uni-muenchen.de](mailto:Johannes.Gnoerich@med.uni-muenchen.de) (J. Gnörich).

<sup>1</sup> Contributed equally.

(76% each). Evaluation of intensity-scaled parametric images resulted in higher sensitivity compared to intensity-scaled static scans (86% vs. 76%) at similar specificity (89% vs. 91%).

**Conclusion:** Visual reading of [<sup>18</sup>F]PI-2620 tau-PET scans demonstrated reliable detection of 4R-tauopathies, particularly when standardized processing methods and early imaging windows were employed. Parametric images should be preferred for visual assessment of 4R-tauopathies.

## 1. Introduction

Tau positron emission tomography (PET) imaging stands as one of the latest additions to the array of tools for in vivo assessment of neurodegenerative proteinopathies (Brendel et al., 2020). Traditionally, the detection of aggregated tau in the brain relied on post-mortem examinations (Litvan et al., 1996) and ante-mortem diagnosis were primarily made through clinical assessments (Höglinger et al., 2017). However, clinical assessments encounter challenges due to symptom overlap of different neurodegenerative diseases like Parkinson's disease (PD), progressive supranuclear palsy (PSP), corticobasal degeneration (CBD), and frontotemporal dementia (FTD) (Höglinger et al., 2017; Williams and Lees, 2009).

Among them, patients with PSP and CBD as well as some patients with FTD are biologically characterized by the aggregation of hyperphosphorylated microtubule-associated four repeat (4R) isoform tau-protein in neurons and glial cells of the brain. PSP clinically manifests with postural instability, falls, and impaired volitional eye movements, often leading to death within 8 years of symptom onset (Rösler et al., 2019). Clinical assessments in PSP and CBD lack sensitivity early in the disease course and exhibit limited specificity for the pathologic entity.

With the rapid progress in tau-targeting therapies, the identification of specific biomarkers for early detection of tau pathology in PSP is imperative (van Eimeren et al., 2019). Early initiation of tau-targeting therapies may prove crucial for effective treatment of neurodegenerative diseases (Boxer et al., 2017). Despite current trials targeting tau in PSP focusing on patients in later disease stages, a validated PSP tau biomarker could facilitate the inclusion of early-stage patients without sacrificing specificity. Molecular biomarkers of tau pathology, particularly tau-PET imaging using [<sup>18</sup>F]PI-2620, demonstrate improved sensitivity compared to structural MRI, providing additive diagnostic information in patients with PSP (Brendel et al., 2020; Messerschmidt et al., 2022).

Besides quantitative analysis of tau-PET there is an urgent need for more clinical practicability to enhance multi-center studies and ensure comparability. Thus, while recognizing efforts to standardize tau-PET scans of 4R-tauopathies through automated quantification methods, the capability of visual assessments to detect 4R-tauopathies needs to be investigated and validated. This validation could expand the clinical applications of tau-PET with regard to 4R-tauopathies, similar to

advancements seen in Alzheimer's disease (AD), where Flortaucipir got FDA-approval for visual reading (Coomans et al., 2023), making it more accessible to physicians and potentially improving patient outcomes.

Therefore, this study aims to comprehensively evaluate the visual assessment of [<sup>18</sup>F]PI-2620 images for diagnosing 4R-tauopathies while developing a straight-forward reading algorithm to enhance objectivity and standardized data reproducibility.

## 2. Methods

### 2.1. Participants

The study included 83 individuals (Table 1), who underwent PET scans employing the second-generation tau-PET radiotracer [<sup>18</sup>F]PI-2620 at the Department of Nuclear Medicine of the LMU Hospital Munich. Only scans comprising the designated scanning time of one hour without motion artifacts were included in the selection sample. An a priori sample size calculation for group discrimination suggested inclusion of  $n = 30$  individuals with 4R-tauopathies (Corticobasal Syndrome (CBS) and PSP) and  $n = 20$  healthy controls. Based on a distribution analysis of clinical diagnoses of [<sup>18</sup>F]PI-2620 PET scans at LMU Hospital Munich, we aimed to additionally include  $n = 20$  patients with AD and  $n = 15$   $\alpha$ -synucleinopathies (PD and Multiple System Atrophy (MSA)) as disease controls to simulate a real-world scenario at a tertiary center.

Prior to tau-PET imaging, participants underwent comprehensive clinical evaluation and received diagnoses at the Department of Neurology with subsequent follow-up examinations. Additionally, a subset of participants underwent lumbar puncture during their visit to LMU University Hospital, Munich, for cerebrospinal fluid (CSF) analysis. CSF biomarker levels, including A $\beta$ 42, A $\beta$ 40, and the A $\beta$ 42/A $\beta$ 40 ratio, were measured using the Innotech ELISA kit (Fujirebio Europe N.V., Belgium). The established cutoff for the A $\beta$ 42/A $\beta$ 40 ratio was set at >5.5%, as per standardized diagnostic procedures at the partnering laboratory. For participants suspected of the AD continuum, biomarker data from CSF and/or  $\beta$ -amyloid PET ([<sup>18</sup>F]-florbetaben or [<sup>18</sup>F]-flutemetamol) were used to confirm or rule out AD as part of the diagnostic process. Patients within the AD continuum included those with either mild cognitive impairment (MCI) or dementia. These patients either had a positive A $\beta$ 42/A $\beta$ 40 ratio or exhibited positive  $\beta$ -amyloid PET results,

**Table 1**

Demographics. Abbreviations: y, years; m, months; MoCa, Montreal Cognitive Assessment; MMSE, Minimal Mental State Examination; UPDRS, Unified Parkinson's Disease Rating Scale; PSPRS, Progressive Supranuclear Palsy Rating Scale; PSP, Progressive Supranuclear Palsy; CBS, Corticobasal Syndrome; AD, Alzheimer's Disease;  $\alpha$ -syn,  $\alpha$ -synucleinopathies; HC = healthy controls.

Group	4-repeat tauopathies	PSP	CBS	AD	$\alpha$ -syn	HC
n	29	21	8	20	15	19
Age, mean (SD), y	75.7 ( $\pm$ 6.4)	76.3 ( $\pm$ 6.4)	74.1 ( $\pm$ 6.2)	76.9 ( $\pm$ 8.1)	65.7 ( $\pm$ 11.1)	65.7 ( $\pm$ 11.1)
Disease Duration, mean (SD), mo	39.0 ( $\pm$ 24.4)	42.4 ( $\pm$ 27.7)	33.3 ( $\pm$ 14.2)	34.8 ( $\pm$ 21.1)	36.8 ( $\pm$ 21.0)	NA
Sex (♀/♂)	11/18	10/11	1/7	10/10	5/10	9/10
CSF A $\beta$ 42/40 mean % (SD)	8.0 ( $\pm$ 1.7)	8.4 ( $\pm$ 1.6)	7.5 ( $\pm$ 1.8)	4.2 ( $\pm$ 1.1)	7.9 ( $\pm$ 2.4)	8.4 ( $\pm$ 1.4)
A $\beta$ -PET +/-	12	6	6	8	NA	11
	0/12	0/6	0/6	8/0	NA	0/11
MoCa score, mean (SD)	22.1 ( $\pm$ 4.7)	22.6 ( $\pm$ 4.3)	20.8 ( $\pm$ 5.9)	18.6 ( $\pm$ 4.5)	18.6 ( $\pm$ 9.4)	28.0 ( $\pm$ 0.0)
MMSE score, mean (SD)	23.3 ( $\pm$ 5.3)	23.9 ( $\pm$ 3.1)	22.4 ( $\pm$ 7.8)	14.0 ( $\pm$ 4.6)	18.0 ( $\pm$ 6.6)	27.5 ( $\pm$ 0.7)
UPDRS score, mean (SD)	37.9 ( $\pm$ 14.8)	40.0 ( $\pm$ 15.0)	32.8 ( $\pm$ 14.9)	39.5 ( $\pm$ 16.7)	38.7 ( $\pm$ 11.7)	NA
PSPRS score, mean (SD)	32.4 ( $\pm$ 13.4)	33.7 ( $\pm$ 14.0)	29.9 ( $\pm$ 12.6)	30.2 ( $\pm$ 12.1)	27.2 ( $\pm$ 12.1)	NA
Follow-Up, mean (SD), mo	39.6 ( $\pm$ 26.1)	43.0 ( $\pm$ 28.0)	30.7 ( $\pm$ 19.0)	21.1 ( $\pm$ 14.5)	38.2 ( $\pm$ 24.6)	NA

both of which met the diagnostic criteria for typical AD (Jack et al., 2011; Dubois et al., 2014). Additionally, early-phase  $\beta$ -amyloid PET (0–10 min) (Völter et al., 2023) and/or tau-PET (0.5–2.5 min) (Beyer et al., 2020) imaging were evaluated as surrogate markers of neuronal loss, highlighting disease-specific perfusion patterns and providing complementary data to the complete A/T/N biomarker framework (Jack et al., 2016). Patients with probable or possible PSP were assessed in accordance with the current diagnostic criteria, with a particular emphasis on closely monitoring disease progression throughout the assessment process (Höglinger et al., 2017). In patients with PSP, disease severity was assessed using the PSP Rating Scale, while cognitive impairment severity was evaluated using the Montreal Cognitive Assessment (MoCA) or Mini-Mental State Examination (MMSE) scores. Participants with  $\alpha$ -synucleinopathies were clinically assessed using state-of-the-art criteria. These included longitudinal observation of clinical trajectories specifically characterized by parkinsonism in PD, as evaluated with the Unified Parkinson's Disease Rating Scale (UPDRS), and autonomic failure in conjunction with parkinsonism or ataxia in MSA (Wenning et al., 2022; Postuma et al., 2015).

Disease duration was defined as the interval between the onset of symptoms and the PET imaging. Follow-up time was defined as the period between the participant's first visit (baseline) and their last visit. Healthy controls were obtained from the ActiGlia study and an ongoing Phase 1 trial.

Two individuals were excluded during the reading process. One patient with clinical PSP was excluded due to concomitant presence of PSP-like tau and Braak III/IV AD-like tau in autopsy. One healthy control was excluded due to  $\beta$ -amyloid positivity. One case of MSA had post-mortem histopathological confirmation of the clinical diagnosis. The final analyzed cohort ( $n = 83$ ) consisted of four distinct diagnostic groups, including age- and largely sex-balanced patients with probable 4R-tauopathy ( $n = 29$ ), AD ( $n = 20$ ),  $\alpha$ -synucleinopathies ( $n = 15$ ), and healthy controls ( $n = 19$ ). A detailed overview of the study groups is provided in Table 1.

## 2.2. Image acquisition and processing

All scans were acquired in a clinical setting on a Siemens Biograph True point 64 PET/CT (Siemens, Erlangen, Germany) or a Siemens mCT (Siemens, Erlangen, Germany). A dynamic PET scan of 60-minutes was performed after slow bolus [ $^{18}\text{F}$ ]PI-2620 i.v. administration. The dynamic brain PET data were acquired in 3-dimensional list-mode over 60-minutes and reconstructed into a  $336 \times 336 \times 109$  matrix (voxel size:  $1.02 \times 1.02 \times 2.03 \text{ mm}^3$ ) using the built-in ordered subset expectation maximization (OSEM) algorithm with 4 iterations, 21 subsets and a 5 mm Gaussian filter. A low-dose CT (0.045 mSv) served for attenuation correction with a tube voltage of 120 kVp, a current-time product of 17 mAs, a single collimation width of 1.2 mm, and a pitch factor of 1.5. No automatic exposure control (CareDose) was employed.

## 2.3. Visual assessment of tau-PET scans

All imaging data were processed using the Hermes Gold LX software. Dynamic scans were examined in transaxial, coronal, and sagittal orientations, with slices presented in the predefined color scale "Kidney" (Mueller et al., 2020; Tezuka et al., 2021) to receive the best visualization of tracer uptake and were then axially corrected. The summed time intervals for analysis were either set from 20 to 40-minutes or from 40 to 60-minutes.

Two different options regarding the intensity were used for visual reading: i) unprocessed sets of raw scans were presented to the reader for self-adjustment (common). ii) a duplicate set was generated including a standardized intensity scaling applied to the scans together with an unprocessed set of scans left for individual adjustment for the reader (Fig. 1).

For intensity scaling, between five and seven regions of interest (ROI) were delineated within transverse slices, specifically in the inferior cerebellar grey matter excluding the dentate nucleus, as a reference tissue (Franzmeier et al., 2022). A volume of interest (VOI) was

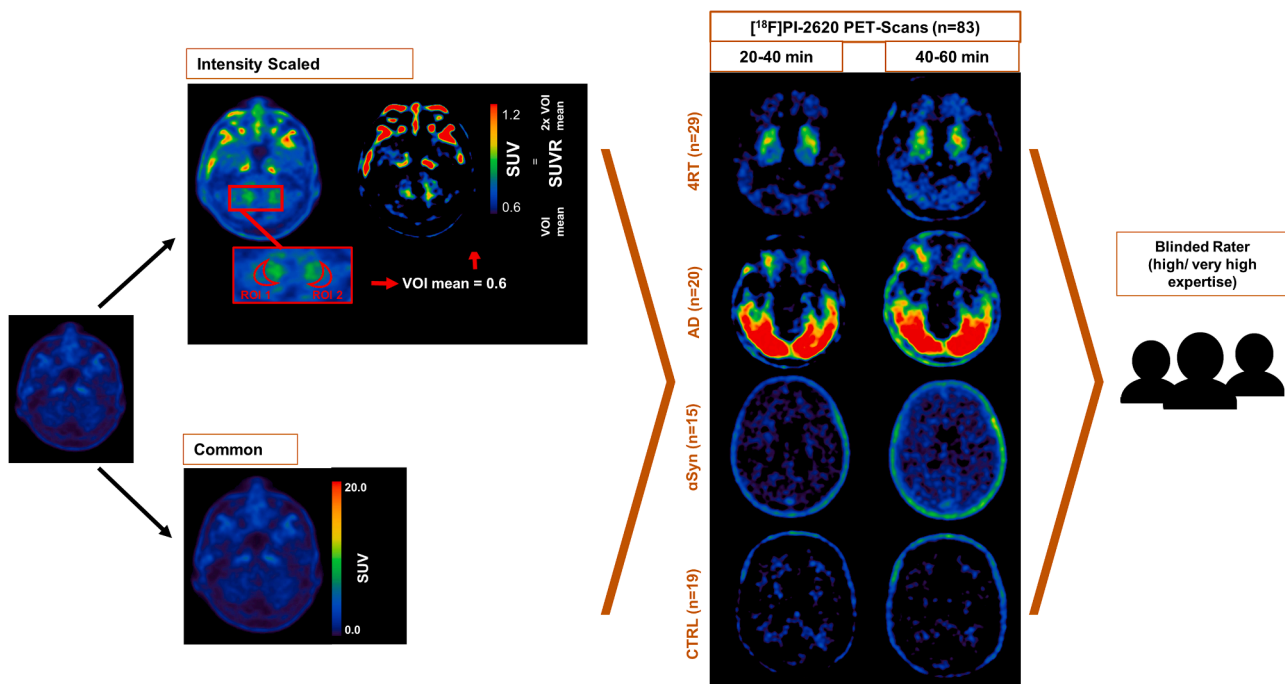


**Fig. 1. Overview of study design.** Visual reading was performed by three readers with high and very high levels of expertise. In total 332 scans were rated across four brain regions (cortex, basal ganglia, midbrain and dentate nucleus) in four different cohorts (4R-tauopathies (4RT), Alzheimer's disease (AD),  $\alpha$ -synucleinopathies (aSyn) and healthy controls (CTRL)) and two different timeframes (20–40-minute and 40–60-minute). No processing (common) and intensity scaling based on cerebellum grey matter reference tissue were applied to each scan and compared across the cohorts, readers, timeframes, and finally compared to parametric images.

subsequently built by aggregating all ROI and the average [ $^{18}\text{F}$ ]PI-2620 standardized uptake value (SUV) was obtained. The average [ $^{18}\text{F}$ ]PI-2620 SUV of the inferior cerebellum was set as the lower limit of the color bar and twice [ $^{18}\text{F}$ ]PI-2620 SUV of the reference region were set as upper limit of the color bar.

All readers were blind to the identity of the scan, and the readers were not given any additional clinical information about the participants, but aware of the included diagnoses in the reading sample. Before conducting the visual assessment, all three readers were provided with detailed instructions and completed training on 10 sets of images, which were independent of the cohort used in this study. A positive score was assigned when an elevated visual [ $^{18}\text{F}$ ]PI-2620 signal was detected, corresponding to a SUVR greater than approximately 1.5. This threshold indicates a tracer uptake that exceeds the cerebellar reference region by more than 50%, highlighting regions of abnormal tau accumulation.

Two primary readers with high (>500 tau-PET reports, 3 years of practice) and very high (>1000 tau-PET reports, 9 years of practice) expertise evaluated all 83 scans under four different conditions (20–40-minute common, 20–40-minute intensity-scaled, 40–60-minute common, 40–60-minute intensity-scaled). A third reader with high expertise (>500 tau-PET reports, 4 years of practice) performed consensus proofreading of all scans with discrepant results between both primary readers. A total of 332 images were rated. In particular, the visual diagnosis was established by assessing tracer accumulation in four distinct brain regions (cortex, basal ganglia with a primary focus on the globus pallidus, midbrain, dentate nuclei). Raters were required to evaluate all these areas to identify any abnormal tracer uptake, classifying it as either indicative of tau-positivity or tau-negativity. The readers were aware of Braak and Kovacs stages (Kovacs et al., 2020; Braak et al., 2006) and had to select one out of three conditions as a combined rating: 4R-tauopathy, Alzheimer's disease-tauopathy, or non-Tauopathy. Non-tauopathy ratings were assumed to include both healthy controls and individuals with  $\alpha$ -synucleinopathies. To compare the value of dynamic and static [ $^{18}\text{F}$ ]PI-2620 scans in visually assessing 4R-tauopathies, we re-evaluated parametric [ $^{18}\text{F}$ ]PI-2620 PET scans of 49 individuals with probable or possible PSP, alongside 12  $\alpha$ -synucleinopathies, 12 AD cases, and 12 controls, from our previously published data (Brendel et al., 2020).

#### 2.4. Statistics

All statistical analyses were carried out with SPSS (version 26.0; IBM) or GraphPad Prism 9 (GraphPad Software, San Diego, USA). For the visual image analysis between the two primary readers, interrater agreement was calculated using the Cohen's kappa  $\kappa$ , and screening quality was evaluated by calculation of sensitivity and specificity. Interrater reliability among all three readers was assessed using Fleiss' kappa ( $\kappa$ ) (Supplemental Figure 1).

### 3. Results

#### 3.1. Visual read performance of different imaging windows and intensity-scaled images for discrimination of 4R-tauopathies

First, we tested the performance of [ $^{18}\text{F}$ ]PI-2620 visual reading for discrimination of 4R-tauopathies from disease controls and healthy controls with binary evaluation of the scan. In the common setting with raw presented images, a sensitivity of 79% (23/29) and a specificity of 78% (42/54) were achieved for detection of 4R-tauopathies in the 20–40-minute frame, accompanied by a moderate agreement between the primary readers (Cohen's kappa:  $\kappa=0.61$ , CI: 0.54–0.69,  $p < 0.001$ ). In direct comparison, the 40–60-minute frame yielded lower sensitivity of 55% (16/29) at higher specificity of 94% (51/54) at moderate interrater agreement ( $\kappa=0.63$ , CI: 0.55–0.70,  $p < 0.001$ ). Intensity-scaled images improved discrimination of 4R-tauopathies from non-4R-tauopathies and indicated a sensitivity of 76% (22/29) and a

specificity of 91% (49/54) for the 20–40-minute frame, at a high interrater agreement between the primary readers ( $\kappa=0.87$ , CI: 0.82–0.92,  $p < 0.001$ ). Intensity-scaled images of the 40–60-minute frame revealed a sensitivity of 62% (18/29) and a specificity of 96% (53/55), yielding a substantial interrater agreement ( $\kappa=0.78$ , CI: 0.72–0.84,  $p < 0.001$ ) (Fig. 2A-B, Supplemental Table 1).

In addition to the primary readers' agreement, interrater reliability was further evaluated using Fleiss' kappa. Notably, the interrater reliability for 4R-tauopathies in the 20–40-minute frame showed substantial agreement in the intensity-scaled setting ( $\kappa=0.74$ , CI: 0.62–0.87,  $p < 0.001$ ). In contrast, the common setting for the same timeframe demonstrated a moderate agreement ( $\kappa = 0.61$ , CI: 0.49–0.74,  $p < 0.001$ ). For the 40–60-minute frame, the intensity-scaled setting exhibited a substantial interrater agreement, with Fleiss' kappa of ( $\kappa=0.70$ , CI: 0.58–0.83,  $p < 0.001$ ). However, the common setting for this timeframe yielded only fair agreement ( $\kappa = 0.42$ , CI: 0.29–0.54,  $p < 0.001$ ) (Supplemental Figure 1).

We further validated our findings by sole consideration of patients with PSP ( $n = 21$ ) from the 4R-tauopathy group. At the same level of specificity, discrimination against the same disease and healthy controls revealed a sensitivity of 81% (+2%) in the 20–40-minute timeframe ( $\kappa=0.62$ , CI: 0.54–0.69,  $p < 0.001$ ) and a sensitivity of 52% (–3%) in the 40–60-minute frame ( $\kappa=0.61$ , CI: 0.53–0.69,  $p < 0.001$ ) of common-scaled images. Regarding the intensity-scaled setting, an ameliorated sensitivity of 81% (+5%) was achieved in the earlier timeframe ( $\kappa=0.85$ , CI: 0.80–0.91,  $p < 0.001$ ), and 67% (+5%) in the later timeframe ( $\kappa=0.78$ , CI: 0.72–0.85,  $p < 0.001$ ) (Supplemental Table 1).

#### 3.2. Visual read performance of different imaging windows and intensity-scaled images for discrimination of Alzheimer's disease

Discrimination of AD against disease controls and healthy controls in common images was achieved at a sensitivity of 90% (18/20) and a specificity of 100% (63/63) for the 20–40-minute frame, with a strong level of interrater agreement ( $\kappa=0.89$ , CI: 0.83–0.95,  $p < 0.001$ ). Using common images of the 40–60-minute frame, there was a similar performance, with strong interrater agreement ( $\kappa=0.89$ , CI: 0.82–0.95,  $p < 0.001$ ), alongside a sensitivity of 85% (17/20) and a specificity of 100% (63/63). Evaluation of intensity-scaled scans revealed similar levels of sensitivity (90%, 18/20) and specificity (100%, 63/63) for discrimination of AD when using the 20–40-minute frame. Here, we observed a perfect agreement between the primary readers ( $\kappa=1.0$ , CI: 1.0–1.0,  $p < 0.001$ ). Similarly, when evaluating the 40–60-minute frame using the intensity-scaled method, we found a sensitivity of 90% (18/20) and a specificity of 100% (63/63) at a significant level of agreement among the readers ( $\kappa=0.89$ , CI: 0.83–0.95,  $p < 0.001$ ) (Fig. 3A-C, Supplemental Table 1). Interrater reliability specifically for 3/4R-tauopathies, demonstrated almost perfect agreement in the intensity-scaled 20–40-minute frame ( $\kappa = 0.93$ , CI: 0.80–1.05,  $p < 0.001$ ). Similarly, the common setting for the same timeframe also showed very high agreement ( $\kappa = 0.91$ , CI: 0.78–1.03,  $p < 0.001$ ). For the 40–60-minute frame, interrater reliability in the intensity-scaled setting exhibited substantial agreement ( $\kappa = 0.78$ , CI: 0.65–0.90,  $p < 0.001$ ), while the common setting showed comparable agreement ( $\kappa = 0.75$ , CI: 0.63–0.87,  $p < 0.001$ ) (Supplemental Figure 1).

#### 3.3. Impact of regional visual rating for detection of 4R-tauopathies vs. non-4R-tauopathies

We analyzed the frequency of tau-positive ratings in each of the predefined target regions in intensity-scaled 20–40-minute frames. Among the primary raters, the basal ganglia were rated positive in 75.9% (Rater1) and 72.4% (Rater2) of the 4R-tauopathy cases. The midbrain, including the substantia nigra, was rated positive in 37.9/34.5% of the cases, followed by the dentate nucleus with 24.1/6.9% positivity and the cortex with 13.8/0.0% positivity (Fig. 4A-B).

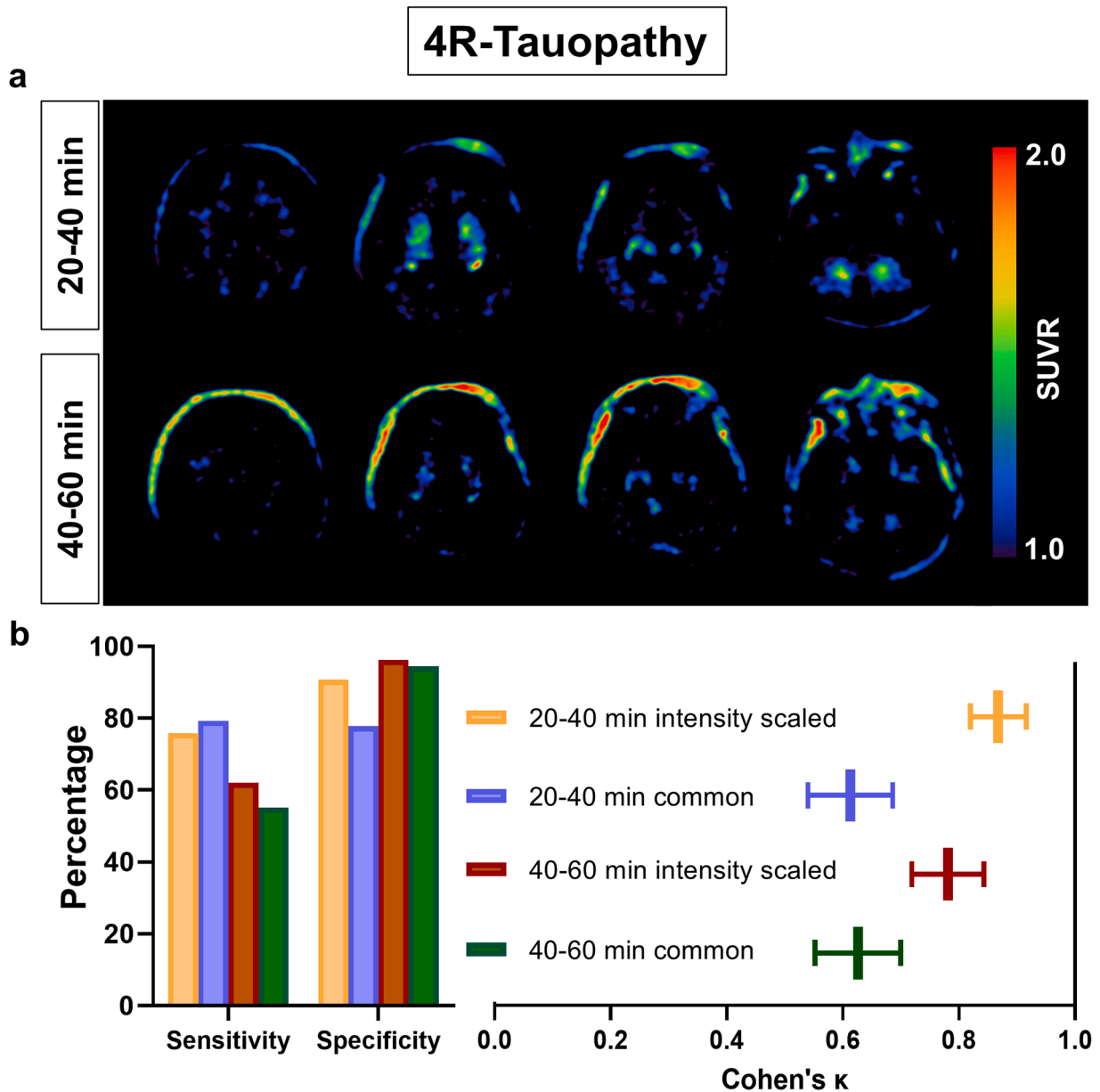


**Fig. 2. Interrater agreement and diagnostic performance of visual tau-PET reading in 4R-tauopathies conducted in different reading settings.** (A) Axial images show a representative patient with 4R-tauopathy consistently rated positive in the 20–40-min frame and negative in the 40–60-min frame. (B) Bar graphs visualize the visual read performance and the box plots depict the interrater Cohen's kappa for both time intervals and processing settings between 4R-tauopathies and non-4R-tauopathies.

Consensus tau-positivity of the basal ganglia was compared to the composite rating of all four predefined target regions in 4R-tauopathies (as shown in Fig. 1). The 20–40-minute frame revealed a sensitivity of 76% for the basal ganglia alone (vs. 76% in the composite rating) and a specificity of 83% (91%) for the intensity-scaled method. The interrater agreement was similar between basal ganglia and composite evaluation ( $\kappa=0.84$ , CI: 0.78–0.90,  $p < 0.001$  vs.  $\kappa=0.87$ , CI: 0.82–0.92,  $p < 0.001$ ). For the 40–60-minute frame, the intensity-scaled method exhibited a sensitivity of 62% (61%) and specificity of 83% (96%), resulting in a substantial interrater agreement ( $\kappa=0.81$ , CI: 0.74–0.88,  $p < 0.001$  vs.  $\kappa=0.78$ , CI: 0.72–0.84,  $p < 0.001$ ). Basal ganglia reading of common images in the 20–40-minute frame showed a sensitivity of 79% (79%) and a specificity of 65% (78%), at a moderate interrater agreement ( $\kappa=0.47$ , 0.38–0.55,  $p < 0.001$  vs.  $\kappa=0.61$ , CI: 0.54–0.69,  $p < 0.001$ ). Similarly, basal ganglia rating of common 40–60-minute images resulted in only moderate interrater agreement ( $\kappa=0.49$ , CI: 0.39–0.59,  $p <$

0.001 vs.  $\kappa=0.63$ , CI: 0.55–0.70,  $p < 0.001$ ), with a sensitivity of 62% (55%) and specificity of 85% (94%) (Fig. 4C-D, Supplemental Table 1).

#### 3.4. Midbrain evaluation increases sensitivity for detection of 4R-tauopathies but decreases specificity

Overall, 24% (7/29) of patients with 4R-tauopathies were rated negative in the basal ganglia based on the consensus principle (20–40-minute, intensity-scaled setting). This subset of patients with 4R-tauopathies underwent further analysis to determine if those patients could be visually classified as 4R-tauopathies due to tracer uptake in single brain regions other than the basal ganglia (cortex, midbrain, dentate nucleus). Here, 2/7 individuals were additionally rated positive in the midbrain but no positive ratings were obtained from the cortex or the dentate nucleus. Next, we evaluated 15 healthy controls with negative consensus read of the whole scan and found midbrain positivity in one case

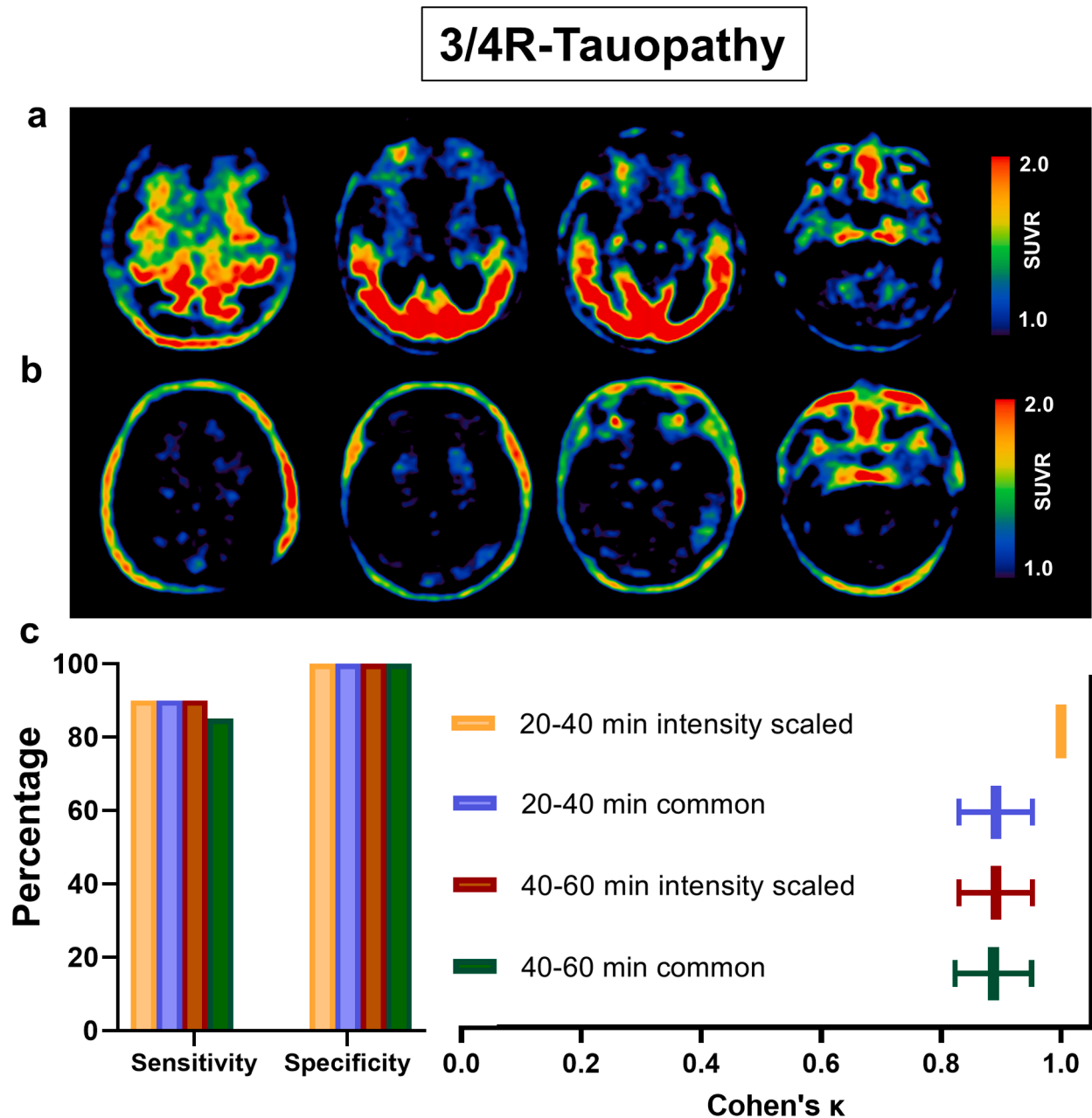


**Fig. 3.** Interrater agreement and diagnostic performance of visual tau-PET reading in patients with AD conducted in different reading settings. (A-B) Two representative [ $^{18}\text{F}$ ]PI-2620-PET scans of patients with a probable 3/4R-tauopathy captured in the 20–40-minute frame: (A) One correctly rated positive by both primary raters, (B) one rated negative by both primary raters. (C) Bar graphs illustrate the visual read performance and box plots depict the interrater agreement for both time intervals and processing settings between patients with AD and non-AD samples.

(Fig. 5A-C). Thus, midbrain evaluation increased sensitivity (+6.9%) and decreased specificity (−5.2%) when considering the whole cohort of 29 patients with 4R-tauopathies and 19 healthy controls.

### 3.5. Visual classification of 4R-tauopathies at the individual-patient level via regional analysis of parametric tau-PET scans

Finally, we compared the evaluated real-world scenario with static [ $^{18}\text{F}$ ]PI-2620 images against parametric images of dynamic PET scans. Specifically, we questioned if a simple basal ganglia assessment also facilitates discrimination of 4R-tauopathies in parametric images. To this end, we re-evaluated parametric [ $^{18}\text{F}$ ]PI-2620 PET-scans of 49 individuals with probable or possible PSP together with twelve individuals with  $\alpha$ -synucleinopathies, twelve individuals with AD and twelve

healthy controls from our previously published data (Brendel et al., 2020; Palleis et al., 2021).

We evaluated tau-positivity in three target regions (basal ganglia, midbrain, dentate nucleus) of distribution volume scaled images. Strikingly, assessment of the basal ganglia revealed a 89% specificity and 86% sensitivity for diagnosing 4R-tauopathies with a high degree of congruency ( $\kappa=0.74$ , CI: 0.66–0.81,  $p < 0.001$ ) between the readers. Sole consideration of the midbrain (sensitivity: 78%, specificity: 63%;  $\kappa=0.40$ , CI: 0.30–0.49,  $p < 0.001$ ) and the dentate nuclei (sensitivity: 94%, specificity: 53%;  $\kappa=0.44$ , CI: 0.36–0.52,  $p < 0.001$ ) only demonstrated a moderate degree of congruency. Finally, to confirm these findings and apply them to our main study group of 4R-tauopathies, we interrogated the false-negative-rated patients and were able to visually unmask tau-positivity, highlighting the ameliorated sensitivity in

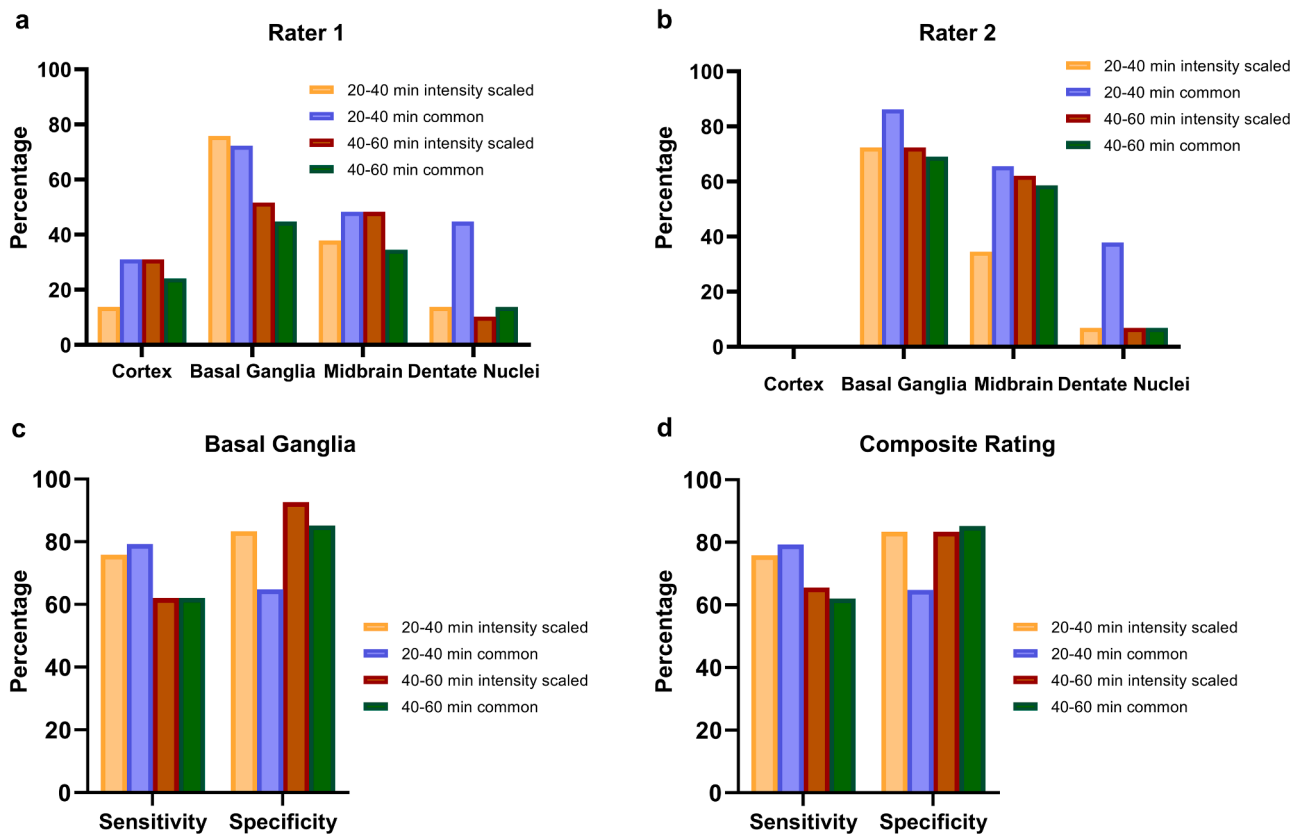


Fig. 4. Comparative analysis of basal ganglia rating against rating of all target regions in 4R-tauopathies. (A-B) Overview of regional rating of both primary readers. (C-D) Bar graphs depict consensus for both time intervals and both processing modalities between 4R-tauopathies and non-4R-tauopathies with solely consideration of the basal ganglia (C) in comparison to consideration of all four target regions (D).

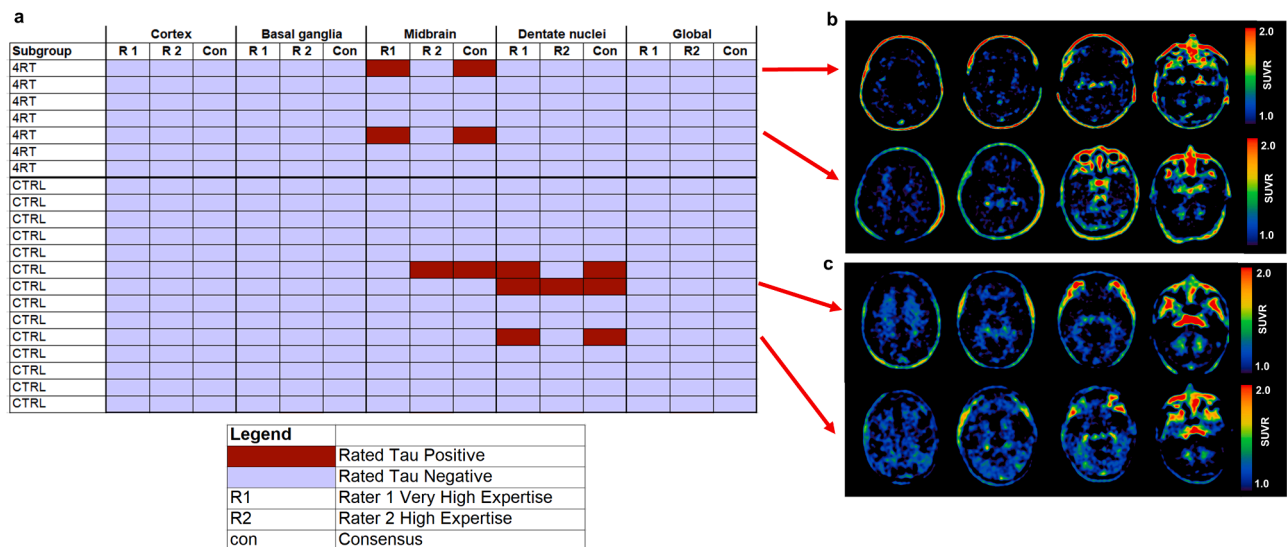


Fig. 5. (A) Heatmap overview of all false-negative rated patients with 4R-tauopathies based on the clinical diagnosis together with true-negative rated healthy controls in the intensity-scaled setting (20–40-minute frame). (B-C) Exemplary axial slices of intensity-scaled [18F]PI-2620-PET scans of false-negative rated patients with 4R-tauopathies (B), true-negative rated healthy controls, although individual regions were rated positive (C).

parametric tau-PET scans (Fig. 6, Supplemental Table 1).

#### 4. Discussion

In this visual reading study, we determined the utility and value of [18F]PI-2620 in visually diagnosing 4R-tauopathies in a clinical setting.

We reached our goal of establishing a straight-forward standardized processing protocol to enhance sensitivity and data reproducibility by i) use of a 20–40-minute static window, ii) use of intensity-scaled images and iii) focus on the basal ganglia as a single target region. Furthermore, we show that parametric imaging is preferred over static windows for sensitive detection of 4R-tauopathies if the specific scenario (i.e.

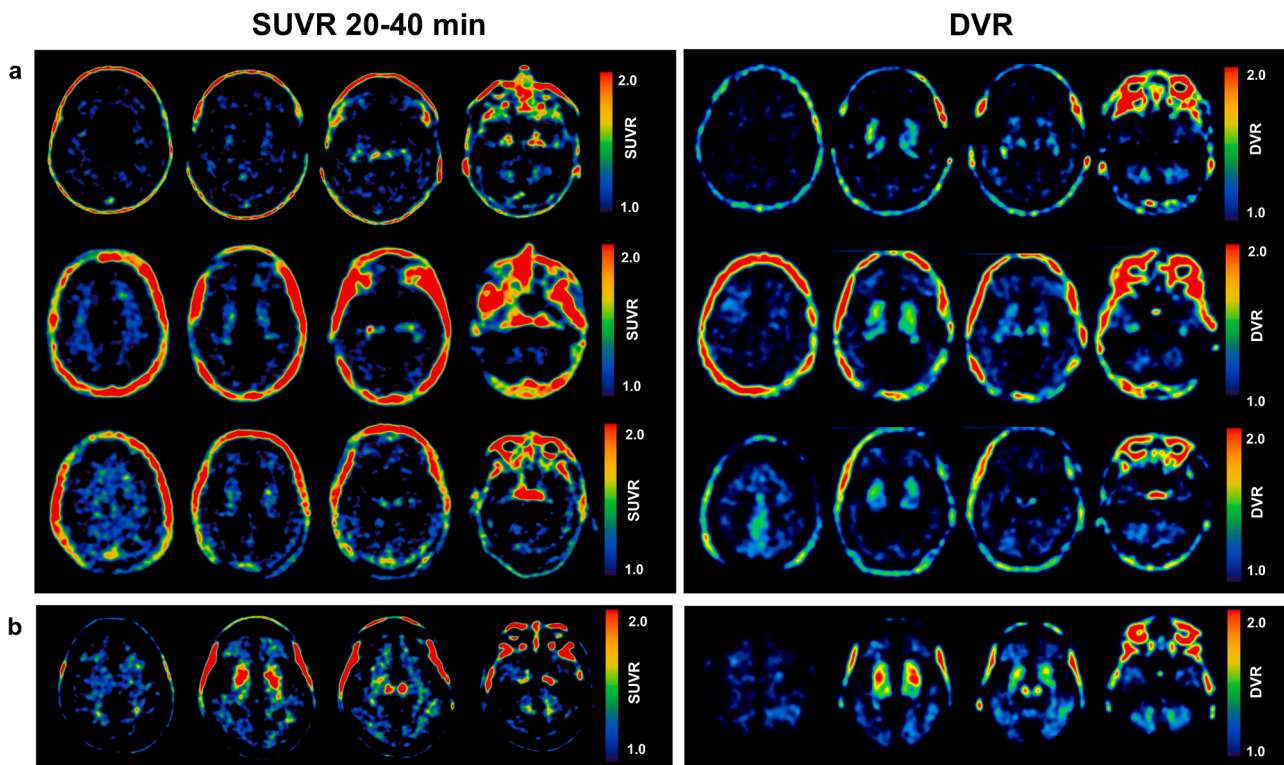


**Fig. 6. Visual evaluation of static versus dynamic tau-PET scans in 4R-tauopathies depicts higher sensitivity in distribution volume ratio (DVR) images. (A) Representative axial [ $^{18}\text{F}$ ]PI-2620 SUVR and DVR images of patients with clinically probable 4R-tauopathies but false-negative visual assessment of SUVR images and true-positive visual assessment of DVR images. (B) An individual patient with clinically probable 4R-tauopathy who was correctly positive rated via SUVR and DVR.**

inclusion into clinical trials vs. clinical work-up) allows higher effort in image acquisition.

The assessment of interrater agreement and the comparison of different reading settings in patients with primary tauopathies versus healthy and disease controls are pivotal for understanding the reliability and efficacy of standardized visual diagnostic methods. We investigated interobserver agreements of [ $^{18}\text{F}$ ]PI-2620-PET scans across two timeframes (20–40; 40–60-minutes) and two reading settings (common and intensity-scaled), providing insights into their diagnostic performance in identifying 4R-tauopathies. First, we observed a greater sensitivity during the earlier time window of 20–40-minutes compared to the 40–60-minute interval, consistent with our previously suggested short imaging protocol in 4R-tauopathies (M. Song et al., 2021). However, the use of 20–40-minutes came at the expense of slightly reduced specificity, likely due to limited washout of nonspecific tracer binding in the target regions of 4R-tauopathies, possibly resulting in false-positive ratings (M. Song et al., 2021). Interestingly, both common and intensity-scaled reading settings exhibited similar sensitivity across both timeframes. Nevertheless, the intensity-scaled setting demonstrated higher specificity and improved inter-rater reliability, particularly notable at 20–40-minutes. We conclude that readers utilizing the common reading setting scrutinize tracer uptake in specific target regions, leading to more sensitive manual adjustments of the images, increasing false-positive ratings, and consequently compromising specificity. Furthermore, manual adjustment introduces potential for subjective variability in image interpretation. Similar to a previously described approach for the visual evaluation of Flortaucipir in MCI and AD (Lu et al., 2021), our standardized intensity-scaled approach for visual image assessment provides a consistent reference framework, ensuring a more uniform evaluation of tracer uptake across different timeframes and among readers. Importantly, the option for manual intensity adjustment remains available to readers, allowing for flexibility. We believe this hybrid approach offers a practical balance between

standardization and physician autonomy, promoting both reproducibility and individualized assessment in clinical practice.

The alignment between the tau-positive rating of the basal ganglia and the overall rating of 4R-tauopathy scans demonstrated high accuracy in terms of sensitivity and specificity. This finding of a sensitive assessment via the basal ganglia read aligns with topology in autopsy since involvement of the basal ganglia is also considered already in stage 1 of the Kovacs classification of PSP (Kovacs et al., 2020).

Importantly, in this study, we focused on the basal ganglia, cortex, midbrain, and dentate nucleus because these regions are closely associated with tauopathies. While AD is primarily linked to cortical tau deposition (Ossenkopppele et al., 2016), 4R-tauopathies, such as PSP, exhibit tau aggregates predominantly in subcortical regions, as shown in various tau-PET imaging studies (Brendel et al., 2020; Schonhaut et al., 2017; Cho et al., 2017; Whitwell et al., 2017). Postmortem histopathological studies have further validated these in vivo findings, confirming the efficacy of these novel tau ligands in specifically detecting tau pathology in PSP target regions (Slemann et al., 2024; Malarte et al., 2023). Additionally, concentrating on these regions enhances diagnostic accuracy, as tau accumulation in the basal ganglia and midbrain has been correlated with disease severity and progression (Brendel et al., 2017). Thus, these areas offer critical insights into distinguishing 4R-tauopathies from other neurodegenerative diseases based on both imaging and neuropathological evidence (Slemann et al., 2024; Dilcher et al., 2024).

Building on these regional distinctions, the combination of disease-specific tau-PET binding patterns and CSF p-tau181 levels has proven to be a reliable biomarker-based algorithm for differentiating AD from 4R-tauopathies. The inclusion of early-phase tau-PET, which serves as a marker for neuronal injury, alongside CSF t-tau, provides additional support in identifying AD (Dilcher et al., 2024). By integrating these early and disease-specific imaging biomarkers, we can enhance diagnostic precision, offering a more refined approach to differentiating



tauopathies in clinical and research settings.

Strikingly, we found that the combined assessment of the basal ganglia, cortex, midbrain, and dentate nucleus did not significantly outperform the sole assessment of the basal ganglia. Furthermore, since only two of the false-negative rated 4R-tauopathy cases were classified as a 4R-tauopathy solely based on an isolated positivity of the midbrain but one additional healthy control was classified positive by the sole evaluation of the midbrain, careful consideration should be given to the inclusion of this target region in the diagnostic process. We attribute the limited specificity to the variable signal due to neuromelanin off-target binding in the substantia nigra (Aguero et al., 2024).

After identifying the basal ganglia as the primary region influencing the readers' final visual ratings, we compared the performance of this region in static versus parametric tau-PET scans. Noteworthy, the sole assessment of parametric DVR in the basal ganglia outperformed the 20–40 intensity-scaled setting in terms of sensitivity while maintaining comparable specificity. Moreover, while conventional SUV scans can be affected by perfusion, perfusion effects are attenuated in DVR scans (Sander et al., 2019), thus ensuring that perfusion deficits in 4R-tauopathies target regions (Katzdobler et al., 2023) do not hamper the visual interpretation of the actual tau load. However, currently dynamic scan sessions typically extend to 60, 75 or even 90 minutes (Brendel et al., 2020; Passamonti et al., 2017), whereas clinical routines often limit patient scans to 20- or 30-minute scan duration. In our study, we opted for a 60-minute dynamic acquisition, which was later reformatted into two static images (20–40 minutes and 40–60 minutes), to balance practical considerations with the benefits of dynamic scanning. Notably, dynamic PET scanning allows for the inclusion of early time frames, offering valuable insights into perfusion deficits, which can act as surrogate markers for neurodegeneration (Beyer et al., 2020). A duration  $\geq 60$  minutes poses challenges, especially for individuals with movement disorders like CBS/PSP.

Considering that the 20–40-minute frame assessment for the intensity-scaled modality demonstrates comparable specificity, our quantitative data suggest the viability of reducing scanning time from 60-minutes to 40-minutes (M. Song et al., 2021), particularly in cases of possible or probable 4R-tauopathies.

The mechanism why early timeframes, such as 20–40-minutes, are more suitable for imaging 4R-tauopathies compared to later short windows, like 40–60-minutes, are not fully understood. Recent neuropathologic and molecular imaging findings have revealed higher binding affinity in presumed tau-positive tissue of 3/4R-tauopathy when contrasted with similar brain regions of 4R-tauopathies (M. Song et al., 2021; Slemann et al., 2024; Malarte et al., 2023). Other studies, however, did not observe significant affinity of tau tracers to tau aggregates in non-AD tauopathies (Aguero et al., 2024) or describe a limited diagnostic potential due to tracer retention in the globus pallidus of healthy controls, as well as a lack of correlation with histopathological validation (Tezuka et al., 2021). Nevertheless, these observations suggest a potentially faster clearance from the target in 4R-tauopathies. Molecular docking simulation pointed out similar differences in 3/4R-tau vs. 4R tau binding of [ $^{18}\text{F}$ ]PI-2620 (Künze et al., 2022). Our visual assessment analysis of 3/4R-tauopathies showed comparable sensitivity across both timeframes, with flawless specificity and no falsely-positive-rated controls. These findings align with previous data indicating reliable visual assessment of 3/4R-tauopathies employing the first-generation tracer [ $^{18}\text{F}$ ]Flortaucipir (Sonni et al., 2020).

The present study addressed the need for standardized processing methods to enhance reproducibility and comparability across centers. While different processing methods showed similar specificity, the standardized method with intensity scaling exhibited significantly higher interrater agreement, suggesting greater reproducibility. Based on these findings, static scans acquired from 20 to 40-minutes or dynamic scans from 0 to 40-minutes can be recommended for clinical practice due to their sufficient sensitivity for 4R-tauopathies and shorter duration, which favors patient compliance as well as offering economic

advantages.

Some limitations should be considered when interpreting our results. The lack of a comparison to post-mortem histopathological validation is a limitation, as misdiagnosis of 4R tauopathies may occur. However, recent data from our group address this limitation by demonstrating a strong correlation between in vivo [ $^{18}\text{F}$ ]PI-2620 PET uptake and post-mortem histopathological validation in deceased PSP patients, underscoring the reliability of this novel tau-PET tracer for accurately detecting tau accumulation in 4R-tauopathies in vivo (Palleis et al., 2021; Slemann et al., 2024). Additionally, the influence of diagnostic certainty based on clinical validation (e.g., suggestive, possible, or probable PSP) may affect our findings. This is particularly important, as the limited availability of biomarker data in a subset of participants may impede the ability to reach a definitive clinical diagnosis.

We intentionally decided to conduct a combined analysis of PSP and CBS cases (4R-tauopathies). The number of CBS cases ( $n = 8$ ) was somewhat limited, and clinical differentiation, as well as topographical overlapping of tau-PET patterns, are limiting factors. To account for potential losses in test accuracy, we successfully demonstrated in a sub-analysis that the sensitivity and specificity remained largely constant when considering PSP cases alone. Although the sample size was determined based on a priori calculations, we acknowledge that the relatively small cohort in our study may limit the generalizability of our findings. Additionally, the slightly increased age difference between the  $\alpha$ -synucleinopathies and healthy controls compared to the 4R-tauopathies must be noted as a limitation.  $\alpha$ -synucleinopathies, including MSA and PD, typically present at a younger age (median onset around 50–60 years) (Wenning et al., 1994; Lees et al., 2009) compared to 4R-tauopathies, which generally present in the late 60s (Nath et al., 2001). Age effects on tau-PET have been observed in some studies, especially in individuals over 80 years (Mormino et al., 2021; Jack et al., 2018). We did not control for age explicitly, as its impact is mainly significant in very elderly cases, which represent only a small subset of 4R-tauopathies in our study. Consequently, while this may introduce a few false positives in the 4R-tauopathy group, the younger age of diagnosis in  $\alpha$ -synucleinopathies reduces the likelihood of significant impact on this group's assessment.

Lastly, differences in reader experience and subjective judgment in image interpretation may introduce potential bias in inter-rater agreement.

## 5. Conclusion

Overall, our findings underscored the reliability of visual [ $^{18}\text{F}$ ]PI-2620 tau-PET reading in diagnosing 4R-tauopathies, with standardized processing methods improving diagnostic accuracy compared to common approaches. These insights contribute to the development of more effective diagnostic protocols and hold promise for enhancing patient care and outcomes in neurodegenerative diseases.

## Data availability

The datasets generated during and/or analyzed during the current study are available from the corresponding author on reasonable request.

## Ethics approval

All procedures performed in studies involving human participants were in accordance with the ethical standards of the institutional and/or national research committee (LMU Munich, application number 17–569) and with the 1964 Helsinki Declaration and its later amendments or comparable ethical standards.

## CRedit authorship contribution statement

**Theresa Bauer:** Writing – original draft, Visualization, Methodology, Investigation, Formal analysis. **Matthias Brendel:** Writing – review & editing, Validation, Methodology, Investigation, Conceptualization. **Mirhind Zaganjori:** Writing – review & editing, Validation, Methodology, Investigation, Conceptualization. **Alexander M. Bernhardt:** Resources, Data curation. **Alexander Jäck:** Resources, Data curation. **Sophia Stöcklein:** Software, Data curation. **Maximilian Scheifele:** Software. **Johannes Levin:** Supervision, Resources. **Thilo van Eimeren:** Writing – review & editing. **Alexander Drzezga:** Writing – review & editing, Funding acquisition. **Osama Sabri:** Supervision, Resources, Conceptualization. **Henryk Barthel:** Writing – review & editing, Supervision. **Robert Perneczky:** Supervision, Funding acquisition. **Günter Höglinger:** Writing – review & editing, Supervision, Funding acquisition. **Nicolai Franzmeier:** Writing – review & editing, Supervision, Project administration, Funding acquisition. **Johannes Gnörich:** Writing – review & editing, Visualization, Supervision, Investigation, Conceptualization.

## Declaration of competing interest

RP received honoraria for advisory boards and speaker engagements from Roche, Eisai, Eli Lilly, Biogen, Janssen-Cilag, Astra Zeneca, Schwabe, Grifols, Novo Nordisk, GSK and Tabuk. AD reports Research Support by: Siemens Healthineers, Life Molecular Imaging, GE Healthcare, AVID Radiopharmaceuticals, Sofie, Eisai, Novartis/AAA, Ariceum Therapeutics and Speaker Honorary/Advisory Boards by: Siemens Healthineers, Sanofi, GE Healthcare, Biogen, Novo Nordisk, Invicro, Novartis/AAA, Bayer Vital, Lilly, Stock by: Siemens Healthineers, Lantheus Holding, Structured therapeutics, Lilly and a patent for 18F-JK-PSMA-7 (Patent No.: EP3765097A1; Date of patent: Jan. 20, 2021).

## Funding sources

GH and RP were funded by the German Research Foundation (DFG) under Germany's Excellence Strategy within the framework of the Munich Cluster for Systems Neurology (EXC 2145 SyNergy – ID 390857198); GH was supported by Rainwater Charitable Foundation (Pre-PSP); European Joint Programme on Rare Diseases (Improve-PSP); Petermax-Müller-Foundation (Etiology and Therapy of Synucleinopathies and Tauopathies); the German Parkinson Society (ProAPS). NF received seed-funding by the German Parkinson Society (DPG). AD was funded by DFG Research Grant DR 445/9–1, and the SFB 1451 Project-ID 431549029 - project C04. RP is supported by the German Center for Neurodegenerative Disorders, the Hirnliga e.V. (Manfred-Strohscheer-Stiftung), the Davos Alzheimer's Collaborative, the VERUM-Foundation, the Robert-Vogel-Foundation, the National Institute for Health and Care Research (NIHR) Sheffield Biomedical Research Centre (NIHR203321), the University of Cambridge – Ludwig-Maximilians-University Munich Strategic Partnership within the framework of the German Excellence Initiative and Excellence Strategy and the European Commission under the Innovative Health Initiative program (project 101132356).

## Supplementary materials

Supplementary material associated with this article can be found, in the online version, at [doi:10.1016/j.neuroimage.2025.121001](https://doi.org/10.1016/j.neuroimage.2025.121001).

## References

Aguero, C., et al., 2024. Head-to-head comparison of [(18)F]-Flortaucipir, [(18)F]-MK-6240 and [(18)F]-PI-2620 postmortem binding across the spectrum of neurodegenerative diseases. *Acta Neuropathol.* 147 (1), 25.  
 Beyer, L., et al., 2020. Early-phase [(18)F]-PI-2620 tau-PET imaging as a surrogate marker of neuronal injury. *Eur. J. Nucl. Med. Mol. Imaging* 47 (12), 2911–2922.

Boxer, A.L., et al., 2017. Advances in progressive supranuclear palsy: new diagnostic criteria, biomarkers, and therapeutic approaches. *Lancet Neurol.* 16 (7), 552–563.  
 Braak, H., et al., 2006. Staging of Alzheimer disease-associated neurofibrillary pathology using paraffin sections and immunocytochemistry. *Acta Neuropathol.* 112 (4), 389–404.  
 Brendel, M., et al., 2017. [(18)F]-THK5351 pet correlates with topology and symptom severity in progressive supranuclear palsy. *Front. Aging Neurosci.* 9, 440.  
 Brendel, M., et al., 2020. Assessment of 18F-PI-2620 as a Biomarker in Progressive Supranuclear Palsy. *JAMA Neurol.* 77 (11), 1408–1419.  
 Cho, H., et al., 2017. Subcortical 18F-AV-1451 binding patterns in progressive supranuclear palsy. *Movement Disorders* 32 (1), 134–140.  
 Coomans, E.M., et al., 2023. Performance of a [(18)F]-Flortaucipir PET Visual Read Method Across the Alzheimer Disease Continuum and in Dementia With Lewy Bodies. *Neurology.* 101 (19), e1850–e1862.  
 Dilcher, R., et al., 2024. Combining cerebrospinal fluid and PI-2620 tau-PET for biomarker-based stratification of Alzheimer's disease and 4R-tauopathies. *Alzheimers. Dement.*  
 Dubois, B., et al., 2014. Advancing research diagnostic criteria for Alzheimer's disease: the IWG-2 criteria. *Lancet Neurol.* 13 (6), 614–629.  
 Franzmeier, N., et al., 2022. Tau deposition patterns are associated with functional connectivity in primary tauopathies. *Nat. Commun.* 13 (1), 1362.  
 Höglinger, G.U., et al., 2017. Clinical diagnosis of progressive supranuclear palsy: the movement disorder society criteria. *Mov. Disord.* 32 (6), 853–864.  
 Jack Jr., C.R., et al., 2011. Introduction to the recommendations from the National Institute on Aging-Alzheimer's Association workgroups on diagnostic guidelines for Alzheimer's disease. *Alzheimers. Dement.* 7 (3), 257–262.  
 Jack Jr., C.R., et al., 2016. A/T/N: an unbiased descriptive classification scheme for Alzheimer disease biomarkers. *Neurology.* 87 (5), 539–547.  
 Jack Jr., C.R., et al., 2018. Longitudinal tau PET in ageing and Alzheimer's disease. *Brain* 141 (5), 1517–1528.  
 Katzdobler, S., et al., 2023. Additive value of [(18)F]-PI-2620 perfusion imaging in progressive supranuclear palsy and corticobasal syndrome. *Eur. J. Nucl. Med. Mol. Imaging* 50 (2), 423–434.  
 Kovacs, G.G., et al., 2020. Distribution patterns of tau pathology in progressive supranuclear palsy. *Acta Neuropathol.* 140 (2), 99–119.  
 Künze, G., et al., 2022. Molecular simulations reveal distinct energetic and kinetic binding properties of [18F]-PI-2620 on tau filaments from 3R/4R and 4R tauopathies. *ACS. Chem. Neurosci.* 13 (14), 2222–2234.  
 Lees, A.J., Hardy, J., Revesz, T., 2009. Parkinson's disease. *The Lancet* 373 (9680), 2055–2066.  
 Litvan, I., et al., 1996. Validity and reliability of the preliminary NINDS neuropathologic criteria for progressive supranuclear palsy and related disorders. *J. Neuropathol. Exp. Neurol.* 55 (1), 97–105.  
 Lu, M., et al., 2021. Aggregated tau measured by visual interpretation of flortaucipir positron emission tomography and the associated risk of clinical progression of mild cognitive impairment and alzheimer disease: results from 2 Phase III clinical trials. *JAMA Neurol.* 78 (4), 445–453.  
 Malarte, M.-L., et al., 2023. Discriminative binding of tau PET tracers PI2620, MK6240 and RO948 in Alzheimer's disease, corticobasal degeneration and progressive supranuclear palsy brains. *Mol. Psychiatry* 28 (3), 1272–1283.  
 Messerschmidt, K., et al., 2022. (18)F-PI-2620 Tau PET Improves the Imaging Diagnosis of Progressive Supranuclear Palsy. *J. Nucl. Med.* 63 (11), 1754–1760.  
 Mormino, E.C., et al., 2021. Tau PET imaging with (18)F-PI-2620 in aging and neurodegenerative diseases. *Eur. J. Nucl. Med. Mol. Imaging* 48 (7), 2233–2244.  
 Mueller, A., et al., 2020. Tau PET imaging with (18)F-PI-2620 in Patients with Alzheimer Disease and Healthy Controls: a First-in-Humans Study. *J. Nucl. Med.* 61 (6), 911–919.  
 Nath, U., et al., 2001. The prevalence of progressive supranuclear palsy (Steele-Richardson-Olszewski syndrome) in the UK. *Brain* 124 (7), 1438–1449.  
 Ossenkoppele, R., et al., 2016. Tau PET patterns mirror clinical and neuroanatomical variability in Alzheimer's disease. *Brain* 139 (Pt 5), 1551–1567.  
 Palleis, C., et al., 2021. Cortical [(18)F]-PI-2620 binding differentiates corticobasal syndrome subtypes. *Mov. Disord.* 36 (9), 2104–2115.  
 Passamonti, L., et al., 2017. 18F-AV-1451 positron emission tomography in Alzheimer's disease and progressive supranuclear palsy. *Brain* 140 (3), 781–791.  
 Postuma, R.B., et al., 2015. MDS clinical diagnostic criteria for Parkinson's disease. *Mov. Disord.* 30 (12), 1591–1601.  
 Rösler, T.W., et al., 2019. Four-repeat tauopathies. *Prog. Neurobiol.* 180, 101644.  
 Sander, C.Y., et al., 2019. Effects of flow changes on radiotracer binding: simultaneous measurement of neuroreceptor binding and cerebral blood flow modulation. *J. Cerebral Blood Flow. Metabol* 39 (1), 131–146.  
 Schonhaut, D.R., et al., 2017. 18F-flortaucipir tau positron emission tomography distinguishes established progressive supranuclear palsy from controls and Parkinson disease: a multicenter study. *Ann. Neurol.* 82 (4), 622–634.  
 Slemann, L., et al., 2024. Neuronal and oligodendroglial but not astroglial tau translates to in vivo tau-PET signals in primary tauopathies. *bioRxiv.* p. 2024.05.04.592508.  
 Song, M., et al., 2021a. Binding characteristics of [18F]-PI-2620 distinguish the clinically predicted tau isoform in different tauopathies by PET. *Journal of Cerebral Blood Flow & Metabolism* 41 (11), 2957–2972.  
 Song, M., et al., 2021b. Feasibility of short imaging protocols for [18F]-PI-2620 tau-PET in progressive supranuclear palsy. *Eur. J. Nucl. Med. Mol. Imaging* 48 (12), 3872–3885.  
 Sonni, I., et al., 2020. Evaluation of a visual interpretation method for tau-PET with (18)F-flortaucipir. *Alzheimers. Dement.* (Amst) 12 (1), e12133.  
 Tezuka, T., et al., 2021. Evaluation of [(18)F]-PI-2620, a second-generation selective tau tracer, for assessing four-repeat tauopathies. *Brain Commun.* 3 (4), fcab190.

- van Eimeren, T., et al., 2019. Neuroimaging biomarkers for clinical trials in atypical parkinsonian disorders: proposal for a Neuroimaging Biomarker Utility System. *Alzheimers. Dement. (Amst)* 11, 301–309.
- Völter, F., et al., 2023. Assessment of perfusion deficit with early phases of [(18)F]PI-2620 tau-PET versus [(18)F]flutemetamol-amyloid-PET recordings. *Eur. J. Nucl. Med. Mol. Imaging* 50 (5), 1384–1394.
- Wenning, G.K., et al., 1994. Clinical features and natural history of multiple system atrophy. An analysis of 100 cases. *Brain* 117, 835–845 (Pt 4).
- Wenning, G.K., et al., 2022. The movement disorder society criteria for the diagnosis of multiple system atrophy. *Movement Disorders* 37 (6), 1131–1148.
- Whitwell, J.L., et al., 2017. [18F]AV-1451 tau positron emission tomography in progressive supranuclear palsy. *Movement Disorders* 32 (1), 124–133.
- Williams, D.R., Lees, A.J., 2009. Progressive supranuclear palsy: clinicopathological concepts and diagnostic challenges. *Lancet Neurol.* 8 (3), 270–279.